Solar-Terrestrial Physics. 2024. Vol. 10. Iss. 1. P. 68–75. DOI: 10.12737/stp-101202410. © 2024
I.V. Korobtsev, M.N. Mishina, Yu.S. Karavaev, M.V. Eselevich, V.E. Goryashin. Published by INFRA-M Academic Publishing House

UDC 520.82, 52-17
DOI: 10.12737/stp-101202410

Received October 19, 2023
Accepted December 06, 2023

PHOTOMETRICAL OBSERVATIONS AND SHAPE MODELING OF SPACE DEBRIS IN MEDIUM EARTH ORBITS

I.V. Korobtsev
Institute of Solar-Terrestrial Physics SB RAS, Irkutsk, Russia, korobtsev@iszf.irk.ru

M.N. Mishina
Institute of Solar-Terrestrial Physics SB RAS, Irkutsk, Russia, mmish@iszf.irk.ru

Yu.S. Karavaev
Institute of Solar-Terrestrial Physics SB RAS, Irkutsk, Russia, y-kar@bk.ru

M.V. Eselevich
Institute of Solar-Terrestrial Physics SB RAS, Irkutsk, Russia, mesel@iszf.irk.ru

V.E. Goryashin
Institute of Solar-Terrestrial Physics SB RAS, Irkutsk, Russia, vgor@iszf.irk.ru

Abstract. The circular medium Earth orbits with a period of about half a day in the inclination range from 50° to 70° are used by various global navigation satellite systems (GNSS), such as GLONASS, GPS, Beidou, Galileo. GNSS operating orbits are one of the important areas in near-Earth space. The information about the space debris (SD) existing in this region and its characteristics is important for risk assessments and mitigation. We report the results of photometrical observations of SD objects in the vicinity of GNSS orbits obtained with the 1.6-meter AZT-33IK telescope of ISTP SB RAS Sayan Solar Observatory in 2018–2023. We show how SD objects existing in this region are distributed relative to GNSS objects. We derive time and phase dependences of the apparent brightness of all measured SD objects. Folded light curves are constructed, rotation periods and their dynamics are determined. The results of modeling the light curve inherent for several SD objects from the GNSS orbital are presented. We suggest a possible space object shape and parameters of proper rotation, which correspond to the observed light curve.

Keywords: space debris, photometrical observations, light curve, modeling.

INTRODUCTION

The number of space debris (SD) objects in near-Earth space is constantly growing. According to the annual report of the European Space Agency [https://www.sdo.esoc.esa.int/environment_report/Space_Environment_Report_latest.pdf], in recent years there has been a significant increase in the number of both launched spacecraft (SC) and cataloged SD. Current estimates (August 11, 2023), made using statistical models [https://www.esa.int/Safety_Security/Space_Debris/Space_debris_by_the_numbers], show that there are 36500 SC objects of size lager than 10 cm in outer space. In case of collision, objects of this size constitute a serious threat to operating SC. Modern optical telescopes can provide monitoring and cataloging of SD objects of sizes from 10 cm in the high-orbit region; however, the accuracy of the orbital parameters of the small-sized objects is usually low due to the absence of regular observations and the significant influence of unmodeled perturbations. Photometrical observations provide an additional source of information about the parameters of proper motion of SD objects, which are necessary for accurate accounting of perturbing forces and to plan space debris removal missions. A number of projects intended to build up databases of SD photometrical light curves are successfully implemented and are publicly available [De Pontieu, 1997; Karpov, 2016; Šilha et al., 2020]. For many years, observations related to monitoring of near-Earth space have been carried out at ISTP SB RAS Sayan Solar Observatory. The purpose of the observations is to obtain trajectory information in order to determine and improve the parameters of orbits of space objects, as well as to gain photometrical information in order to identify other characteristics (parameters of proper rotation, possible shape and size). The main types of observational photometrical information are the apparent brightness as a function of time and phase angle. The apparent brightness of a space object depends on its size, shape, surface material, orientation, distance to the observer, etc. Modeling SD light curves and comparing them with experimental data provide information about possible characteristics of reflecting surfaces and object parameters of rotation around the center of mass.

This paper presents photometrical observations of SD objects in the vicinity of orbits of global navigation satellite systems (GNSS) GLONASS, GPS, Galileo, and Beidou. The constellations of satellites considered are located in near-circular orbits with a period of about half a day in the altitude range 18000–25000 km with inclinations from 50 to 70°. Currently there is almost no information on the characteristics of SD objects unrelated to spacecraft launches in these orbits. We present light curves and the SD brightness as a function of phase angle, as well as the results of shape modeling of a space object, and the parameters of its proper rotation, which correspond to the light curve shape inherent to several observable SD objects.

1. PHOTOMETRICAL OBSERVATIONS

1.1. Objects of observations

Data on parameters of the orbits of active and decommissioned satellites, rocket bodies (RB), and objects related to launches is regularly updated in the open catalog of the North American Aerospace Defense Command (NORAD) [https://www.space-track.org]. At the same time, data on the parameters of SD orbits is limited in this catalog, for example, it contains orbital data on only one large SD object No. 43381 (international No. 2008-020C) in the vicinity of GNSS. PJSC "IAC Vympel" publishes materials that contain a significant amount of information about orbital parameters of high-orbiting SD objects [http://spacedata.vimpel.ru/ru]. This source provides data on 29 SD objects in the vicinity of GNSS orbits: 16 objects are located in the vicinity of GLONASS orbits; 3, in the vicinity of Galileo; 10, in the vicinity of Beidou and GPS. In total, 411 objects together with SD have been cataloged in the vicinity of GNSS orbits: 281 active and decommissioned satellites, 101 rocket bodies, and various mission-related objects. Figure 1 illustrates distribution of all the objects over orbital planes.

The average area-to-mass ratio (AMR) for half of the SD objects ranges from 0.1 to 1 m^2/kg; for the remaining ones, from 1 to 10 m^2/kg, which is significantly higher than the characteristic value for SC and rocket bodies generally not exceeding 0.03 m^2/kg. This means that the orbital dynamics of these objects is significantly affected by solar radiation pressure poorly accounted in modeling [Bakhtigaraev et al., 2016]. The average catalog brightness of most objects ranges from 16 to 20 magnitude. Figure 2 shows distributions of SD objects by AMR and mean catalog brightness.

1.2. Equipment and observational technique

All observations presented in this work were made with the 1.6-meter AZT-33IK telescope of ISTP SB RAS Sayan Solar Observatory in 2018–2023. The AZT-33IK telescope has a Ritchey — Chrétien optical system with a focal reducer (F=7 m). The field of view with an Andor Neo 5.5 sCMOS camera (2160×2560 pixels) is ~7×8 arcmin, the angular pixel size is 0.185 arcsec. The main measurements are carried out in a 4×4 binning mode with a resulting scale of 0.74 arcsec/pixel. Photometrical observations are made both using wideband filters BVRI of the Johnson—Cousins system and in integrated light without a filter.

Photometric measurements of SD light curves were performed in the observation mode without a filter with series duration from 20 min. The exposure time and duration of the series were selected depending on the object brightness and the expected period of its rotation. The observations were planned so that to cover as wide range of phase angles as possible in order to plot the brightness phase angle dependences. All photometrical observations involved obtaining calibration images: flat field frames in the twilight sky and dark current frames for each operating exposure. The primary reduction of astronomical observations (subtraction of the averaged dark frame, division into a normalized averaged flat field) was made according to a standard procedure with the Apex-II software package [Devyatkin, 2010]; for their further astrometrical and photometrical processing, along with Apex-II we applied our own programs for automatic processing of observational data.

The light curves of objects are graphs of the apparent magnitude along the Y-axis and the time from the beginning of observations along the X-axis. Each light curve is tested for the presence of a periodic signal by frequency analysis methods. For the initial analysis of the periodic component, we use the fast Fourier transform [Deeming, 1975]. The obtained period is verified by the Lafler — Kinman data folding method [Lafler, Kinman, 1965], and the folded light curve for the rotation period is plotted. Examples of the light curve of object No. 67505 and its associated folded light curve are given in Figure 3.

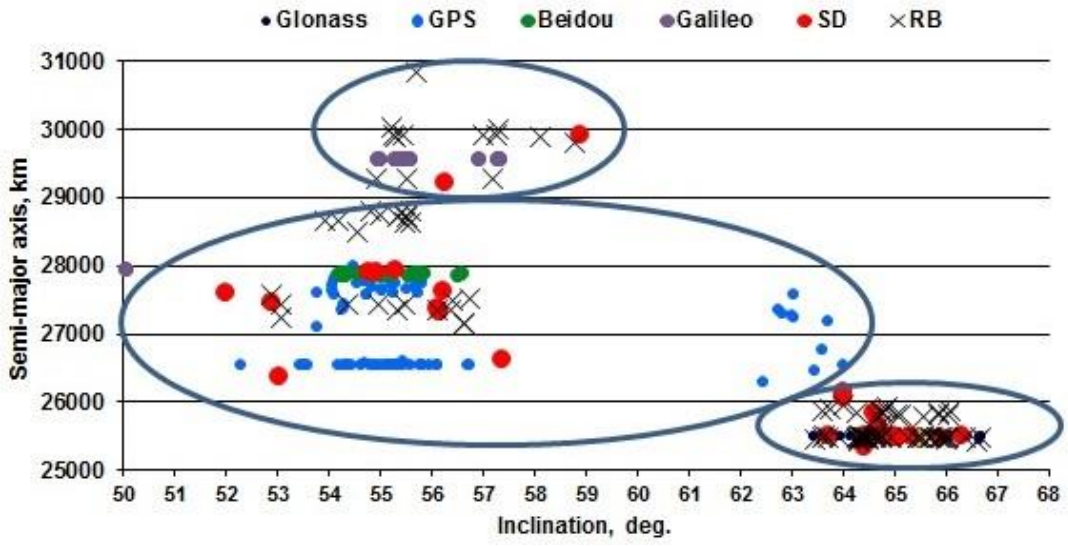

Figure 1. Distribution of cataloged space objects in the vicinity of active GNSS

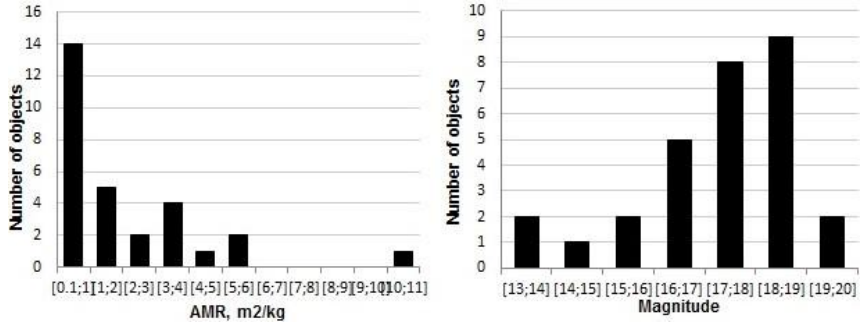

Figure 2. Distribution of cataloged SD objects by AMR (left) and brightness (right)

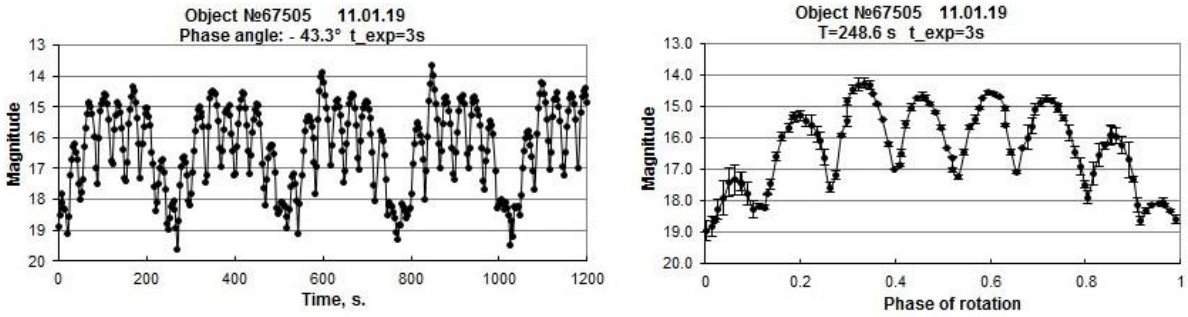

Figure 3. Light curve of SD object No. 67505 (left) and folded light curve for the rotation period (right)

1.3. Light curve analysis results

A sufficient number of measurements made it possible to obtain photometrical characteristics of objects — the average brightness and the amplitude of its variation, characteristic features of the brightness variation, the rotation period and its dynamics, brightness phase angle dependence.

Characteristics of all the objects measured are presented in Table. Table columns show:

- the object number in the PJSC "IAC Vympel" bulletin;
- the proper rotation period (in the form of a range since the period may change over time);
- the average brightness reduced to a zero phase angle and a distance of 20000 km;
- the maximum amplitude of brightness variation;
- the average effective area-to-mass ratio (AMR);
- size estimated by the diffusely-reflecting sphere model with an albedo of 0.15.

Characteristics of SD objects in the vicinity of GNSS orbits

Object No.	Period, s	Average brightness reduced to 0° phase angle, magnitude.	Amplitude, magnitude	AMR, m^2/kg	Estimated size, cm
slow-rotating in the vicinity of GLONASS					
67403	472–437	17.5	4.0	0.39	17
67506	315–340	16.5	4.5	0.38	25
67505	242–291	16.5	5.0	0.44	25
67513	73–109	17	4.0	0.45	20
67410	66	17.5	3	0.34	17
67408	52–39	16.5	3.5	0.31	25
67517	234–219	16	3.5	0.55	35
68908	83	17.5	3.5	1.9	17
68207	26.8	13	4.0	0.13	140
fast-rotating in the vicinity of GLONASS					
67515	–	16.5	1.5	0.77	25
67516	–	17	1.5	1	20
67508	–	12.5	1.0	0.08	175
in the vicinity of Beidou and GPS					
76113	–	18	2.0	0.31	15
75118	26.8	18	2.5	0.05	15
74920	–	17.5	2	0.23	17
72011	–	18.5	1	3.2	12
in the vicinity of Galileo					
85800	120–170	13	4.5	2.9	140
82700	3.2	14	2.0	5.7	100

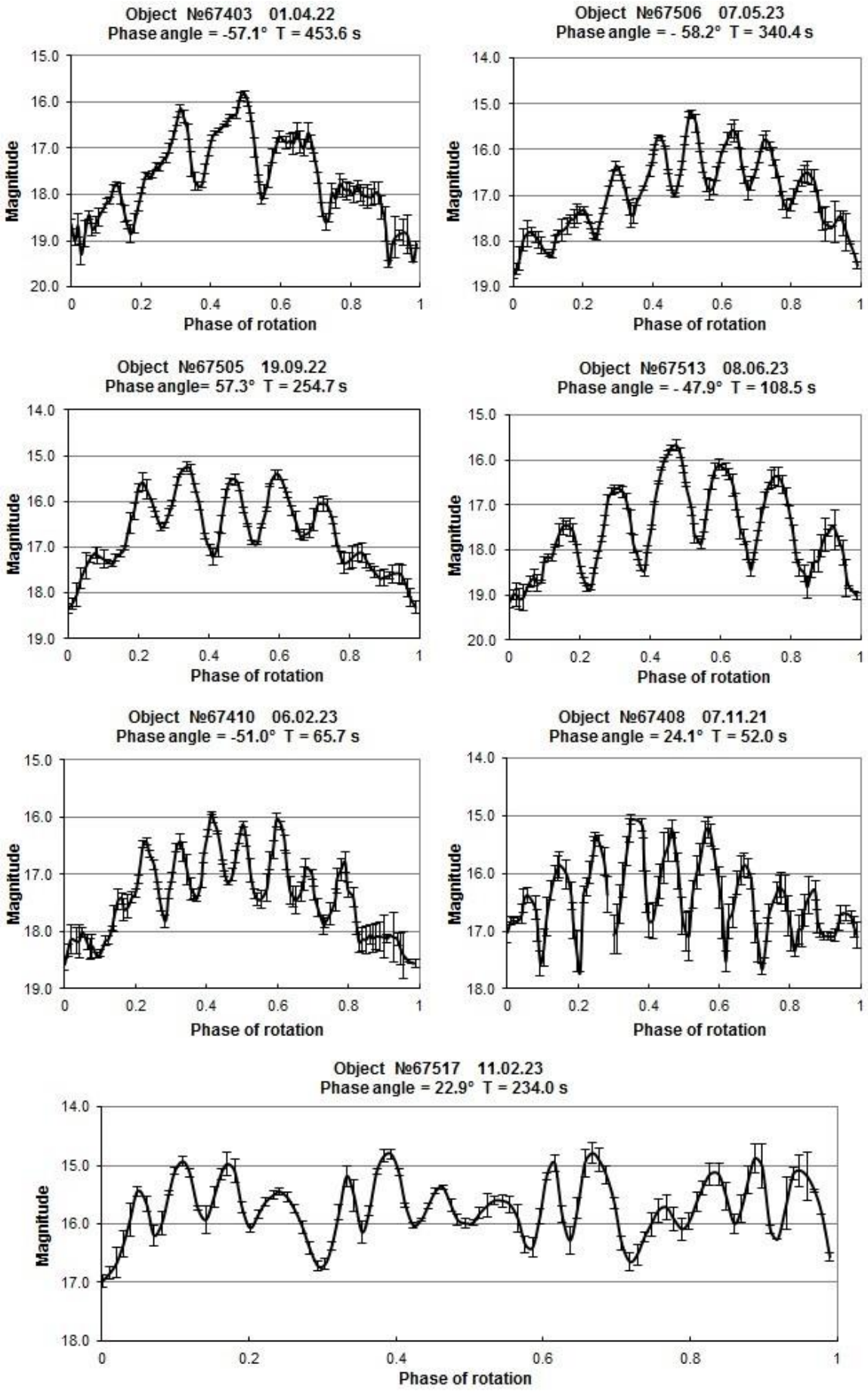

Figure 4. Folded light curves of objects with close photometrical characteristics in the vicinity of GLONASS

All twelve SD objects observed in the vicinity of GLONASS show periodic brightness variations indicating a rotation. According to rotation rate, objects are conditionally divided into slow-rotating with rotation periods from several tens to several hundred seconds, and fast-rotating with periods of several seconds (periods of these objects are not reliably determined due to insufficient time resolution).Seven slow-rotating objects in the vicinity of GLONASS (highlighted in color in Table) have similar characteristics: AMR~0.4 m^2/kg, average brightness ~17 magnitude, no brightness phase angle dependence. The light curves of all these objects have a characteristic shape with several peaks for a period (from five to fourteen) and deep minima between periods, which indicates that the objects have a complex shape and rotation. Figure 4 shows folded light curves for seven objects with similar characteristics.

Two more objects with relatively slow rotation (No. 68908, No. 68207) are located away from the main GLONASS constellation, in the orbital region with rocket bodies. Both objects rotate with periods of several tens of seconds. The average brightnesses and the shapes of the folded light curves of these objects differ significantly. Object No. 68908 is one with the smallest brightness, its brightness at minima reaches the 19th magnitude, has a mirror-symmetric folded light curve relative to the middle of the rotation phase. Object No. 68207 exhibits bright flashes that reach the 11th magnitude at their maximum. The size of object No. 68908 is 17 cm; the size of object No. 68207 is 140 cm (as estimated from the average brightness by the diffuse-reflecting sphere model with a 0.15 albedo). Folded light curves of objects No. 68908 and No. 68207 are presented in Figure 5.

There were four SD objects in the vicinity of closely spaced GPS and Beidou and two objects in the vicinity of Galileo. The objects in the vicinity of the GPS and Beidou constellations are the smallest of the observed ones — 12–17 cm, whereas the objects in the vicinity of Galileo are quite large — 100 and 140 cm. We determine rotation periods and plot folded light curves only for two objects — No. 75118 and No. 85800 (Figure 6).

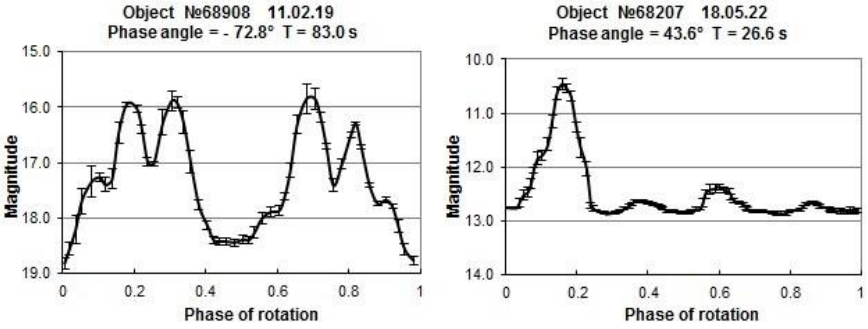

Figure 5. Folded light curves of objects located away from the main GLONASS constellation

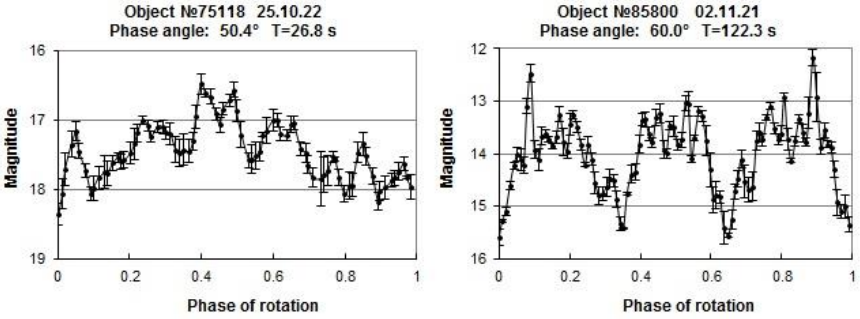

Figure 6. Folded light curves of objects in the vicinity of GPS (left) and Galileo (right)

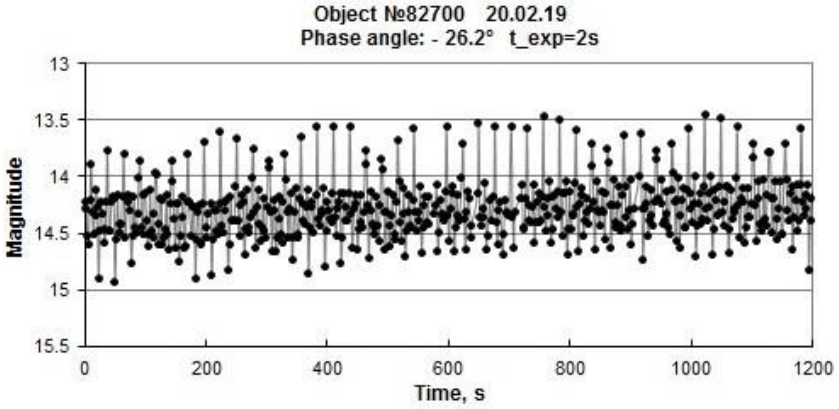

Figure 7. Folded light curve of object No. 82700 with the aliasing effect

The remaining objects, whose rotation period could not be found due to insufficient time resolution, exhibit rapid brightness variations. Observing such objects requires an exposure time of a few seconds such that an acceptable signal-to-noise ratio will not be achieved. The light curves of these objects often exhibit the aliasing effect that occurs when the sampling period is close to the period of brightness variation. The light curve of a fast-rotating object with the aliasing effect is shown in Figure 7.

1.4. Results of the analysis of brightness phase angle dependences

For the objects whose observations cover a large range of phase angles, we have plotted the brightness, reduced to a distance of 20000 km, as a function of phase angle. Examples of the brightness phase angle dependences are given in Figures 8 and 9. Most objects showing slow rotation do not have a well-defined brightness phase angles dependence: the average brightness of objects remains almost constant at all phase angles, which corresponds to objects with a predominant mirror reflection. In some cases (see object No. 67513 in Figure 8), the average brightness increases with increasing phase angle. Fast-rotating objects mainly have brightness phase angle dependence characteristic of objects with diffuse reflection, with the average brightness increasing at small phase angles (see Figure 9).

2. SD SHAPE MODELING

This section presents the results of modeling of the radiation reflected from freely rotating SD objects, which have light curves of a similar shape (see Figure 4) — with multiple maxima for a period and deep minima between periods. Free rotation of an object was modeled using the Matlab mathematical package [https://www.mathworks.com/products/matlab.html]. We have taken the inertial system XYZ with the origin in the center of the rotating body. The light source is located at infinity and radiates along the Z-axis. The XZ plane contains a vector directed to the observer. The second system, $x_1x_2x_3$ with the origin at the center of inertia of the rotating body, is related to the rotating body, and the axes x_1, x_2, x_3 coincide with the main moments of inertia I_1,I_2,I_3 respectively. The body orientation relative to XYZ is described by the Eulerian angles φ, ψ, and θ. Numerical integration of Eulerian equations (1), (2) in the absence of external moments gives the position of the object in the inertial reference system XYZ [Landau, Lifshitz, 2004]:

$$\begin{cases} I_1 \dfrac{d\omega_1}{dt} + (I_3 - I_2)\omega_2\omega_3 = 0, \\ I_2 \dfrac{d\omega_2}{dt} + (I_1 - I_3)\omega_1\omega_3 = 0, \\ I_3 \dfrac{d\omega_3}{dt} + (I_2 - I_1)\omega_2\omega_1 = 0. \end{cases} \quad (1)$$

$$\begin{cases} \dfrac{d\varphi}{dt} = \dfrac{\omega_1 \sin\psi + \omega_2 \cos\psi}{\sin\theta}, \\ \dfrac{d\psi}{dt} = \omega_3 - \dfrac{\cos\theta(\omega_1 \sin\psi + \omega_2 \cos\psi)}{\sin\theta}, \\ \dfrac{d\theta}{dt} = \omega_1 \cos\psi - \omega_2 \sin\psi, \end{cases} \quad (2)$$

where ω_1, ω_2, ω_3 are projections of angular velocities in the inertial reference system.

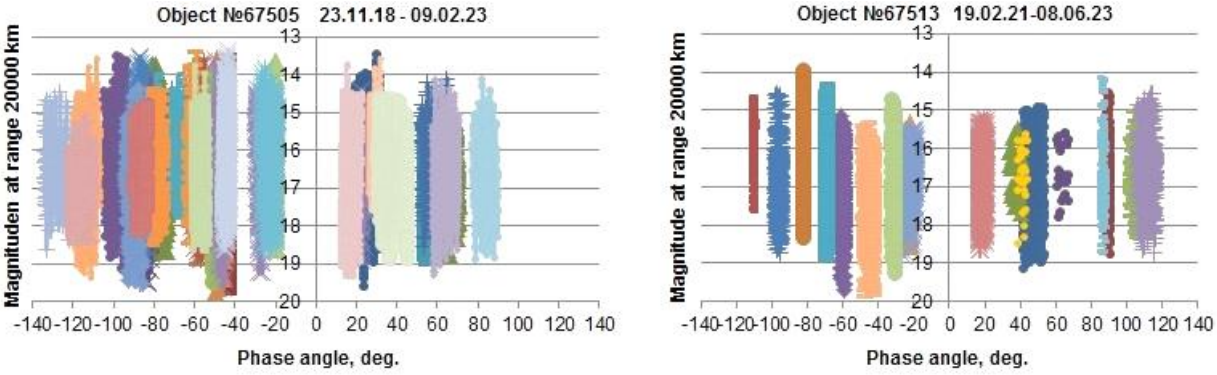

Figure 8. Phase dependences of slow-rotating SD objects

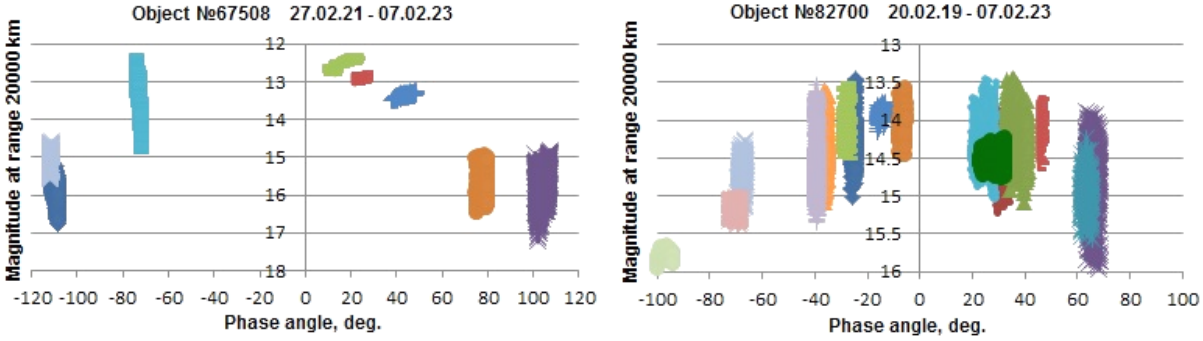

Figure 9. Phase dependences of fast-rotating SD objects

For a freely rotating rigid body, the sum of the angular momentum and the rotational energy determined by ratios (3) and (4) should be constant:

$$I_1\omega_1 + I_2\omega_2 + I_3\omega_3 = const, \quad (3)$$

$$\frac{I_1\omega_1^2}{2} + \frac{I_2\omega_2^2}{2} + \frac{I_3\omega_3^2}{2} = const. \quad (4)$$

If $I_1 > I_2 > I_3$, the body rotation around an axis parallel to the intermediate moment of inertia I_2 will be unstable. If at the initial moment the angular velocity deviates slightly from the axis, the angle of deviation will increase rapidly and instead of a simple uniform rotation around a constant direction the body will begin to perform a disorderly looking tumbling such that the vector of instantaneous angular velocity constantly changes direction. This unstable rotation is also called the Dzhanibekov effect [Murakami et al., 2016].

For the modeling we have chosen an object with the main axes of inertia fitting the condition $I_1 > I_2 > I_3$ rotating around the axis parallel to I_2. The initial position and shape of the simulated SD object are depicted in Figure 10.

The object with a mass m=0.45 kg is parallelepiped of length L=0.45 m, width W=0.40 m, and height B=0.20 m.

One of the conditions for choosing such parameters was an approximate equality between AMR of the simulated object and AMR of the observed objects. The main moments of inertia for this model are determined in accordance with system of equations (5):

$$\begin{cases} I_1 = \dfrac{m\left(W^2 + B^2\right)}{12}, \\ I_2 = \dfrac{m\left(L^2 + B^2\right)}{12}, \\ I_3 = \dfrac{m\left(W^2 + L^2\right)}{12}. \end{cases} \quad (5)$$

The initial angular velocity [rad/s] was given by the vector ω_0=[0.05, 0.2, 0], where [ω_1, ω_2, ω_3] are projections of ω_0. The initial orientation of the body in the inertial reference system corresponds to the Eulerian angles [0, 0, 0]. The phase angle of the Sun — observer object was 30°. We dealt with the diffuse reflection of light from faces of rotating light-gray object (0.8). The background around the object is black.

The graphs in Figure 11 show that the angular velocity components ω_2, ω_3 periodically change sign in the inertial reference system, whereas the total angular momentum and the rotational energy remain constant, which confirms the correctness of the solutions obtained.

Next, an animation of the motion of the simulated object was created. The animation results were recorded in a video file, the video file was subdivided into frames, using the freely distributed utility VirtualDub [https://www.virtualdub.org]. In each received frame, the brightness values of all pixels were summed; the results were presented in magnitude format and recorded in a text file. Then, a model light curve was plotted (see Figure 12, left).

It is clear that from the simulation we could obtain a light curve close in shape to the observed light curves of SD objects. This shape of the light curve can be explained by the different sizes of faces. Minima with a period of ~100 s correspond to the moments when the angular velocity changes sign. At these moments, the main contribution to the reflected radiation is made by the apparent face that has a minimum area. Since there is no a priori information about the objects of observation, in this work we did not aim to accurately account for the

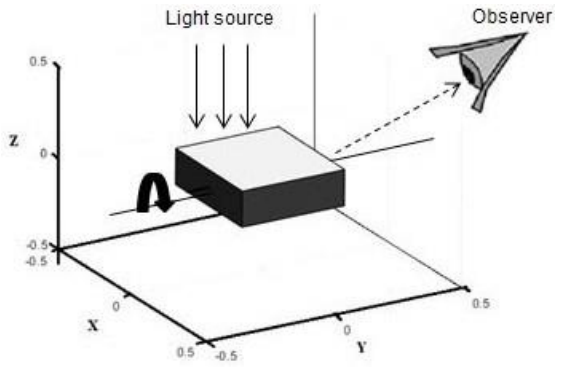

Figure 10. Shape and initial position of the simulated SD object

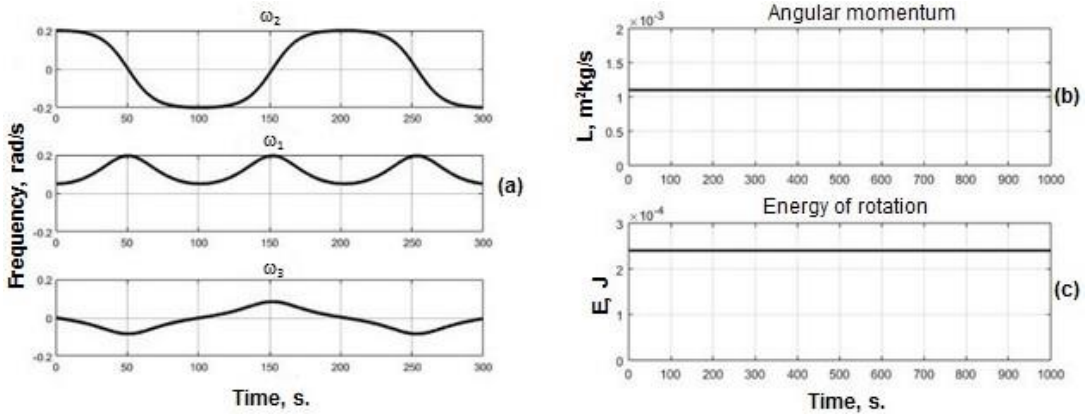

Figure 11. Temporal dynamics of components of angular velocity (*a*), angular momentum (*b*), and rotational energy (*c*) of the simulated object

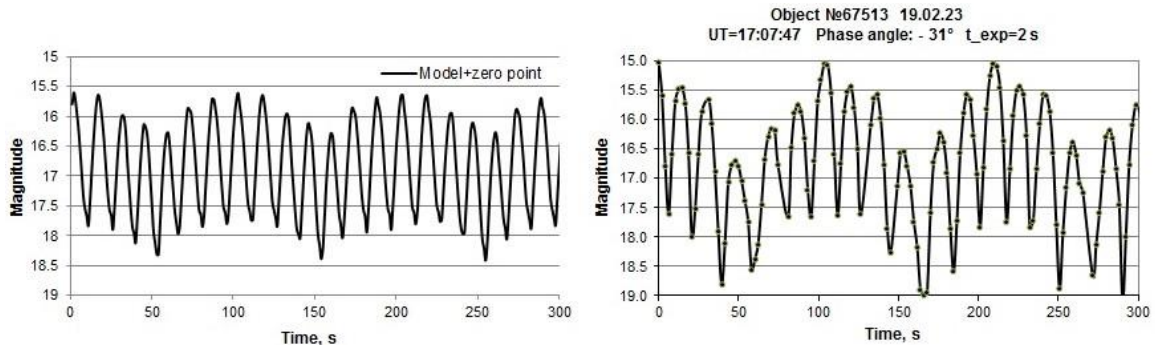

Figure 12. Light curve of the simulated SD object (left) and the light curve of object No. 67513 (right)

magnitude of the apparent brightness of the simulated object, but only modeled the geometric shape of the object and its motion around the center of mass.

CONCLUSION

Space debris poses a serious threat to missions in near-Earth space. In this work, we have obtained and analyzed photometrical observations of space debris in the vicinity of GNSS orbits. We have determined photometrical characteristics of 18 SD objects, and have estimated their sizes, using the diffusely-reflecting sphere model and measured average brightnesses. Seven objects with close photometric characteristics and hence similarly-shaped light curves have been identified in the vicinity of GLONASS orbits. We have modeled the shape and mode of proper rotation of a SD object corresponding to the light curve characteristic of these seven objects. The multi-peak structure of the light curve with deep minima indicates the complex nonstationary rotation of objects, in which the angular velocity components periodically change sign in the inertial reference system (tumbling of the object). The combination of photometrical observations and model results provides new information about the expected shape and size of a SD object, as well as about parameters of proper rotation.

The work was financially supported by the Ministry of Science and Higher Education of the Russian Federation. The results were obtained using the equipment of Shared Equipment Center «Angara» [http://ckp-rf.ru/ckp/3056].

REFERENCES

Bakhtigaraev N.S., Levkina P.A., Chazov V.V. Empirical model of motion of space debris in the geostationary region. *Solar System Res*. 2016, vol. 50, iss. 2, pp. 130–135. DOI: 10.1134/S0038094616020027.

Deeming T.J. Fourier analysis with unequally-spaced data. *Astrophys. Space Sci.* 1975, vol. 36, iss. 1, pp. 137–158. DOI: 10.1007/BF00681947.

De Pontieu B. Database of photometric periods of artificial satellites. *Adv. Space Res*. 1997, vol. 19, iss. 2, pp. 229–232. DOI: 10.1016/S0273-1177(97)00005-7.

Devyatkin A.B., Gorshanov D.L., Kupriyanov V.V., Vereshchagina I.A. “Apex-I” and “Apex-II” software packages for astronomical CCD observations processing. *Astronomicheskii vestnik* [Astronomical Bulletin]. 2010, vol. 50, no. 1, pp. 74–87. (In Russian).

Karpov S., Katkova E., Beskin G., Biryukov A., Bondar S., Davydov E., et al. Massive photometry of low-altitude artificial satellites on MINIMEGA-TORTORA. *Revista Mexicana de Astronomia y Astrofisica (Serie de Conferencias)*. 2016, vol. 48, pp. 112–113.

Lafler J., Kinman T.D. An RR Lyrae star survey with the Lick 20-inch astrograph II. The calculation of RR Lyrae periods by electronic computer. *Astrophys. J. Supplement*. 1965, vol. 11, pp. 216–222. DOI: 10.1086/190116.

Landau L.D., Lifshitz E.M. *Teoreticheskaya fizika. T. I.: Mekhanika*. [Theoretical Physics. Vol. I.: Mechanics]. Moscow, Nauka Publ., 2004, 224 p. (In Russian).

Murakami H., Rios O., Impelluso T.J. A theoretical and numerical study of the Dzhanibekov and tennis racket phenomena. *Journal Applied Mechanics*. 2016, vol. 83, iss. 11, 111006. 10 p. DOI: 10.1115/1.4034318.

Šilha J., Krajčovič S., Zigo M., Toth J., Žilkova D., Zigo P., et al. Space debris observations with the Slovak AGO70 telescope: Astrometry and light curves. *Adv. Space Res*. 2020, vol. 65, iss. 8, pp. 2018–2035. DOI: 10.1016/j.asr.2020.01.038.

URL: https://www.sdo.esoc.esa.int/environment_report/Space_Environment_Report_latest.pdf (accessed August 20, 2023).

URL: https://www.esa.int/Safety_Security/Space_Debris/Space_debris_by_the_numbers (accessed August 11, 2023).

URL: https://www.space-track.org (accessed August 20, 2023).

URL: http://spacedata.vimpel.ru/ru (accessed August 7, 2023).

URL: https://www.mathworks.com/products/matlab.html (accessed January 12, 2022).

URL: https://www.virtualdub.org (accessed January 12, 2022).

URL: http://ckp-rf.ru/ckp/3056/ (accessed March 12, 2023).

Original Russian version: Korobtsev I.V., Mishina M.N., Karavaev Yu.S., Eselevich M.V., Goryashin V.E., published in Solnechno-zemnaya fizika. 2024. Vol. 10. Iss. 1. P. 74–82. DOI: 10.12737/szf-101202410.

How to cite this article

Korobtsev I.V., Mishina M.N., Karavaev Yu.S., Eselevich M.V., Goryashin V.E. Photometrical observations and shape modeling of space debris in medium Earth orbits. *Solar-Terrestrial Physics*. 2024. Vol. 10. Iss. 1. P. 68–75. DOI: 10.12737/stp-101202410.